Journal of Applied Physics

High pressure-induced phase transition in nanocrystalline iron confined by single-walled carbon nanohorns

Cite as: J. Appl. Phys. **131**, 055901 (2022); https://doi.org/10.1063/5.0074420
Submitted: 08 October 2021 • Accepted: 14 January 2022 • Published Online: 02 February 2022

Yanli Nan, Liuming Lei, Zihan Zhang, et al.

Journal of Applied Physics ARTICLE scitation.org/journal/jap

High pressure-induced phase transition in nanocrystalline iron confined by single-walled carbon nanohorns

Cite as: J. Appl. Phys. **131**, 055901 (2022); doi: 10.1063/5.0074420
Submitted: 8 October 2021 · Accepted: 14 January 2022 ·
Published Online: 2 February 2022

Yanli Nan,[1,a)] Liuming Lei,[1] Zihan Zhang,[1] Bo Li,[2,b)] and Lei Su[3,4,c)]

AFFILIATIONS

[1]School of Material Science and Engineering, Shaanxi Key Laboratory of Nano Materials and Technology, Xi'an University of Architecture and Technology, Xi'an 710055, China
[2]School of Materials Science and Engineering, Xi'an University of Technology, Xi'an 710048, China
[3]Key Laboratory of Photochemistry, Institute of Chemistry, University of Chinese Academy of Sciences, Chinese Academy of Sciences, Beijing 100190, China
[4]Center for High Pressure Science and Technology Advanced Research, Beijing 100094, China

[a)]**Author to whom correspondence should be addressed:** nanyl@xauat.edu.cn
[b)]**Electronic mail:** libo930@xaut.edu.cn
[c)]**Electronic mail:** leisu2050@iccas.ac.cn

ABSTRACT

This study examines the high-pressure structural properties of nanocrystalline Fe confined by single-walled carbon nanohorns (SWCNHs) and SWCNHs (filled with Fe nanoparticles) named Fe-filled SWCNHs up to a pressure of 21.8 GPa. In detail, the Fe-filled SWCNHs did not undergo a special structural transformation at up to 21.8 GPa, except the partial irreversible amorphization of graphene sheets forming the core part above ~18 GPa. Cubic Fe (bcc Fe) and Fe_3O_4 coexisted simultaneously in the Fe-filled SWCNHs. The Fe encapsulated by the SWCNH underwent a reversible transformation from bcc Fe to a hexagonal Fe (hcp Fe) at 11.7 GPa and reversed to bcc Fe at 6.2 GPa with a width of the domain of coexistence of bcc hcp of the order of 5 GPa. Due to the effect of the special tubular confinement of the SWCNHs, the high-pressure behavior of Fe confined by them exhibited a sharp contrast to that of Fe confined by carbon nanotubes. In comparison to the bulk bcc Fe, hcp Fe, and Fe_3O_4, these nanocrystallines confined by SWCNHs had higher compressibility than their bulk phases. Fe_3O_4 did not exhibit any phase transformation until 21.8 GPa, where this was similar to the results of bulk Fe_3O_4.

I. INTRODUCTION

The encapsulation of various nanometal crystals in carbon nanotubes (CNTs) and single-walled carbon nanohorns (SWCNHs) has been widely studied under a high hydrostatic pressure. This is because new and unique physical properties and phase transformations emerge on these nanometal crystals and the host CNTs/SWCNHs.[1–3] For example, several remarkable features and interesting results have been obtained on Fe-filled CNTs. Karmakar *et al.* showed that phases of cubic Fe (bcc Fe) and Fe_3C confined by multi-walled CNTs (MWCNTs) have higher compressibility than their bulk phases.[4] The phase transformation from bcc to hcp in bcc Fe does not occur up to a pressure of 20 GPa. Iso-structural phase transitions occur in MWCNTs and Fe_3C confined by MWCNTs but do not occur in bulk Fe_3C and pristine MWCNTs. They used these results to show that bcc Fe-filled MWCNTs without Fe_3C do not exhibit any structural transformation up to a pressure of 9 GPa.[5] Although the bulk modulus of the encapsulated bcc Fe is similar to that of bulk Fe, bcc Fe confined by MWCNTs does not undergo a phase transformation until 19 GPa. However, previous reports[6,7] have shown that bulk and bare nanocrystalline Fe can undergo the transformation from bcc to hcp in the range of pressure from 10 to 14 GPa. And hcp Fe can transform back to bcc Fe below 11.9 GPa. The explanations offered for these behaviors of Fe-filled CNTs are not yet clear. More research on such systems is

needed to gain further insight into the high-pressure behavior of Fe encapsulated by nanocarbon materials.

SWCNHs have more remarkable structures than CNTs even though they are nanotubular. Through their self-assembling mechanism, thousands of cylindrical nanotubulars are formed at spherical SWCNHs with a "dahlia-like" feature.[8] The core of the SWCNHs is composed of disordered graphene sheets.[9] According to our previous report, SWCNHs exhibit phase transition behaviors that are similar to those of single-walled CNTs in terms of their high-pressure Raman spectra and x-ray diffraction (XRD) under 20 GPa.[10,11] The nanocrystalline confined by the SWCNH shows many unique phase transitions and characteristics that are not observed in CNTs. Urita *et al.* discovered that the high-pressure phase structure of KI encapsulated by SWCNHs can undergo spontaneous growth from B1 to B2 owing to the tubular confinement of the SWCNHs.[12] On the contrary, bulk solid KI requires a pressure higher than 1.9 GPa for the phase transition from B1 to B2. Li *et al.* reported that orthorhombic sulfur confined by SWCNHs exhibit different behaviors from that of bulk sulfur under high pressure caused by the confinement effect of SWCNHs.[3] Fe nanoparticles encapsulated by CNHs can be synthesized by one-step arc discharge in liquid nitrogen according to Sano's reports.[13] Fe-filled SWCNHs have attracted considerable attention in catalytic activity for the esterification of palmitic acid.[14] Thus, it is important to determine the behaviors and phase transformations of nanocrystalline-Fe confined by SWCNHs in contrast to that of Fe-filled CNTs. However, few experimental reports on nanocrystalline Fe confined by SWCNHs have been published.

In this study, we focus on the high-pressure behavior of Fe-filled SWCNHs produced by the one-step arc-discharge method[13] to investigate the components, phase transitions, bulk moduli, and directions of deformation of crystalline Fe by using transmission electron microscopy (TEM), x-ray photoelectron spectroscopy (XPS), and synchrotron-based angle-dispersive x-ray diffraction (XRD) with the help of the Rietveld analysis using GSAS software. The unique characteristics of the phase transitions revealed by these analyses are reported.

II. EXPERIMENTAL DETAILS

Fe-filled SWCNHs were produced by using N_2 gas in the arc-in-water method based on the reports by Sano *et al.*[13,14] A hole (1 mm diameter, 60 mm depth) was drilled axially in a graphite rod used as an anode (6.1 mm) into which an Fe wire with a diameter of 0.8 mm was inserted. The arc discharge was generated at 100 A between the anode and a holey graphite cathode (10 mm, hole diameter, 25 mm, hole depth) submerged in water through the injection of N_2 gas (8 l/min).

We characterized the morphologies of all samples by using a high-resolution transmission electron microscope (HRTEM) (JEOL, JEM-2010F). X-ray photoelectron spectroscopy (XPS, Shimadzu, Ultra DLD) was used to analyze the elements and structures. The peak of C1 s was defined at 284.6 eV as the internal standard. An XRD (Rigaku, RINT2100) with Cu-Ka radiation at a power of 40 kV and current of 40 mA was used to obtain the phase and crystal structure of the samples.

The high-pressure structural transformations of the SWCNHs were performed by using the diamond anvil cell (DAC) technique combined with *in situ* synchrotron-based radiation x-ray diffraction (XRD). A DAC device with a size of the diamond culet of 500 μm was used to generate pressures of ~21.8 GPa. The 4W2 High-Pressure Station of the Beijing Synchrotron Radiation Facility in China was used to perform the high-pressure XRD experiments. Monochromatic radiation at 0.6199 Å with a spot of size $10 \times 31\ \mu m^2$ was used to collect the data. Two-dimensional imaging plate records were transformed to one-dimensional diffraction profiles by the radial integration of diffraction rings using FIT2D software.[15] Le-Bail profile fitting in GSAS software was used to examine pressure-induced variations in the lattice parameters.[16]

III. RESULTS AND DISCUSSION

A typical TEM image of the Fe-filled SWCNHs is shown in Fig. 1(a). The peripheral SWCNH aggregates were composed of a large number of individual CNHs and have "dahlia-like" structures with a diameter of 40–50 nm. As shown in Fig. 1(c), each cylindrical nanotubular unit consisted of a cone-shaped tip with a cone angle of ~20° and a diameter of 2–5 nm. In addition, we can see that the nanocrystalline Fe was wrapped in the individual CNHs. It should be noted that the pentagonal and heptagonal defects are the indispensable condition to form the cone-shaped tip. Figure 1(d) shows a schematic illustration of individual CNHs filled with Fe nanoparticles with cone-shaped tips distributed pentagons and heptagons. Actually, some Fe nanoparticles are wrapped by nanotubular units [in Fig. 1(g)] and graphite layers [in Fig. 1(g)] surrounded by nanotubular units. As a result, we can see that the structure of Fe confined by SWCNHs has a big difference from the structure of Fe confined by CNTs. The diameter of the Fe particles was mainly concentrated in the range of 2–7 nm (by measuring over 500 particles) [in Fig. 1(b)]. Figures 1(e) and 1(f) show HRTEM images of the Fe nanocrystal. The lattice spacings of 0.252 and 0.202 nm corresponded to the (311) interplanar distances of Fe_3O_4 and the (110) interplanar distances of bcc Fe, respectively.

The XRD pattern of the Fe-filled SWCNHs under ambient conditions is depicted in Fig. 2. The patterns of the Pnma space group of Fe_3C, the $Fd\bar{3}m$ space group of Fe_3O_4, and the $Im\bar{3}m$ space group of bcc Fe can be indexed on this pattern. Although the two strongest peaks of Fe_3C were clearly observed in the XRD patterns, they were difficult to distinguish because the peaks of Fe_3C were very close to those of graphite and bcc Fe. Furthermore, the lattice spacing of Fe_3C could be barely observed in the HRTEM images. Therefore, the existence and the content of Fe_3C are needed to be further confirmed by XPS and other analyses. The *d*-spacings of the bcc Fe and Fe_3O_4 as calculated by the XRD patterns were similar to those obtained from observations of the HRTEM images.

Figure 3(a) shows three major peaks of the Fe-filled SWCNHs at ~284.5, 532.7, and ~710.0 eV denoted by C1s, O1s, and Fe 2p, respectively.[17,18] Oxygen was present for two reasons: the exposure of the samples to air and the process of arc discharge from the boiling water. In our experiments, the high-resolution spectra of the 2p peak of Fe were fitted into six components centered at 706.9, 707.8, 710.1, 711.5, 719.1, and 720.2 eV [see Fig. 2(b)], which were

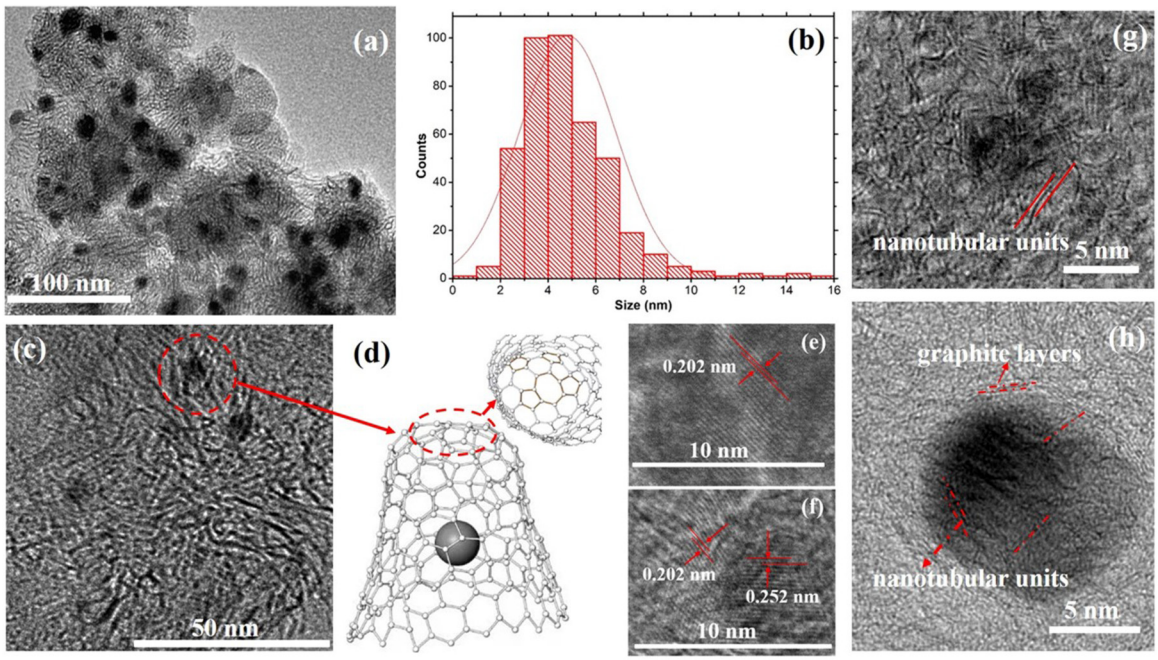

FIG. 1. (a) Typical morphology of Fe-filled SWCNHs. (b) The size distribution of the nanocrystalline Fe. (c) The HRTEM image of Fe confined by individual CNHs. (d) Schematic illustration of Fe-filled CNHs. (e) and (f) Lattice fringes of Fe confined by SWCNHs showing the *d*-spacing of nanocrystalline Fe. (g) and (h) HRTEM images of Fe confined by SWCNHs.

assigned to Fe^{0+}, Fe_3C, iron oxide $Fe2p_{3/2}$, and iron $Fe2p_{1/2}$,[19,20,21] suggesting that Fe, Fe_3C, and iron oxide were produced simultaneously during arc discharge. The relative ratios of Fe and iron oxide were 52% and 47%, respectively, and the Fe_3C phase constituted

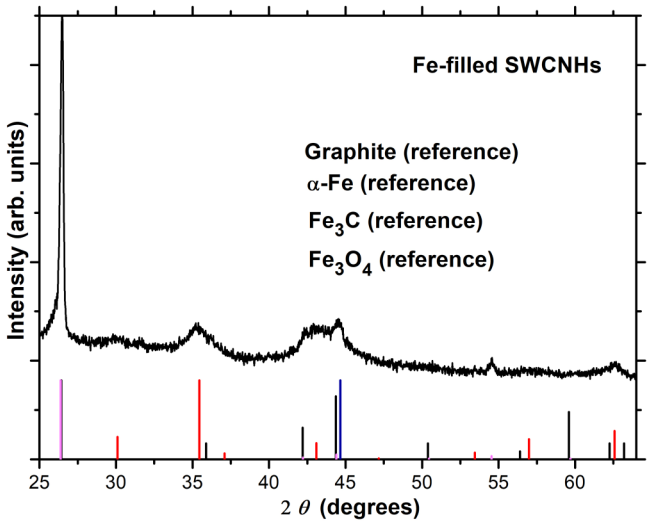

FIG. 2. The XRD results of Fe-filled SWCNHs in ambient conditions.

less than 1%. These results are consistent with those analyzed by the Rietveld refinement using GSAS software on the results of the synchrotron and are explained below.

The high-pressure behaviors of nanocrystalline Fe confined by the SWCNHs at a few representative pressures are presented by its x-ray diffraction patterns in Fig. 4. It should be noted that the synchrotron x-ray diffraction patterns became much wider owing to the smaller particle size under high pressure. With increasing pressure, the 2θ degrees of the nanocrystalline Fe tended to up-shift, suggesting that its *d*-spacings had decreased under high hydrostatic pressure. Up to 11.7 GPa, two new synchrotron x-ray diffraction peaks for hcp Fe appeared at (101) and (102), indicating that the nanocrystalline bcc Fe had begun to transform into hcp Fe.

To confirm the accuracy of the overall results, the profile analysis is provided here using the Le-Bail profile.[22] The ambient pressure pattern (Fig. 5) was indexed on the primitive bcc Fe and Fe_3O_4 unit cells with $Im\bar{3}m$ and $Fd\bar{3}m$ space groups, respectively. The x-ray diffraction pattern recorded at 11.7 GPa (Fig. 5) matched the hexagonal structure obtained using the space group $P6_3/mmc$ (194). The values of the weighted profile factor (R_{wp}), expected profile factor (R_{exp}), and reduced chi-square (χ^2) were 8%, 10%, and 1.3 for 0.07 GPa and 10%, 9%, and 1.8 for 11.7 GPa, respectively.

In the stage where bcc Fe and hcp Fe coexisted, the XRD peaks of the remaining bcc Fe widened drastically and weakened in intensity when hcp Fe appeared, indicating that the transformed zones had also induced a large plastic deformation on the

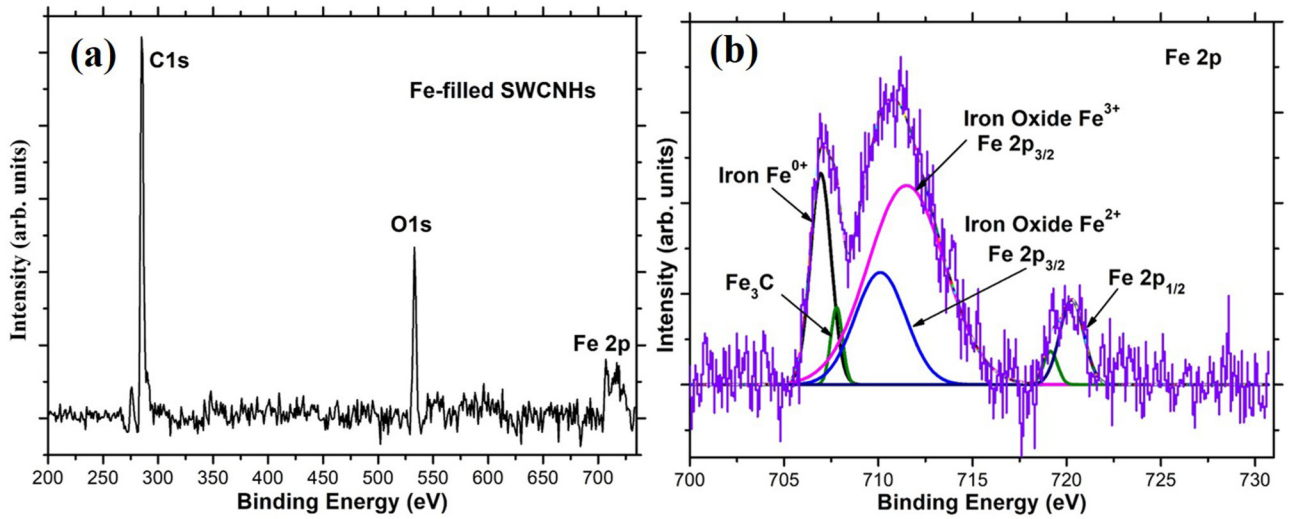

FIG. 3. (a) XPS spectrum of Fe-filled SWCNHs. (b) The high resolution peak for Fe 2p.

remaining, untransformed bcc Fe. The phase of hcp Fe persisted until 21.8 GPa, the highest pressure considered in this study. Note that bcc Fe confined by the SWCNHs underwent a phase transformation from bcc to hcp above 11.7 GPa, different from the Fe confined by CNTs that did not undergo any phase transition until 20 GPa.[4,5] Upon decompression, the diffraction patterns of hcp completely disappeared at 6.2 GPa while those of bcc Fe reappeared, implying the reversible nature of hcp-to-bcc transformation. It should be noted that the pressures of the transitions from bcc to hcp and from hcp to bcc were not performed with high precision because the measurements were carried over increments in pressure.

The synchrotron XRD patterns and the profile analysis imply that the encapsulated Fe_3O_4 did not undergo any phase transition up to the highest pressure in our experiment, where this is similar to the results for bulk Fe_3O_4.[23,24] Furthermore, under hydrostatic

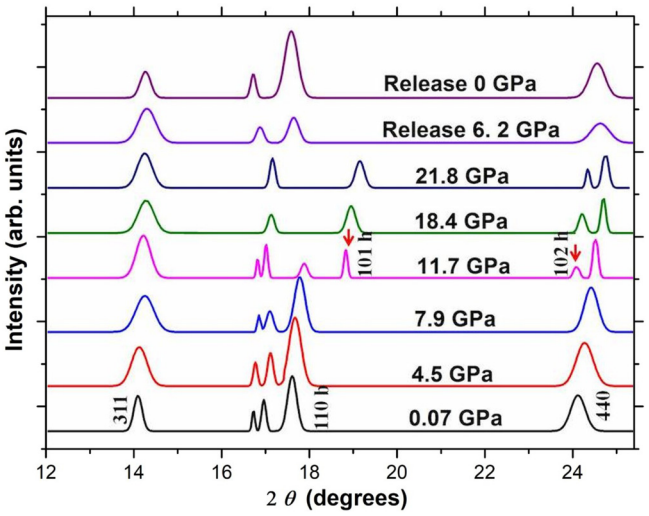

FIG. 4. The synchrotron x-ray diffraction patterns of nanocrystalline Fe confined by SWCNHs at a few representative pressures (b for the bcc phase; h for the hcp phase). The peaks around at 17° maybe aroused by graphite carbon. At 0.07 GPa, the planes of (311) and (440) represent Fe_3O_4, and that of (110) represents the bcc Fe. At 11.7 GPa, the arrows represent the peak of hcp Fe.

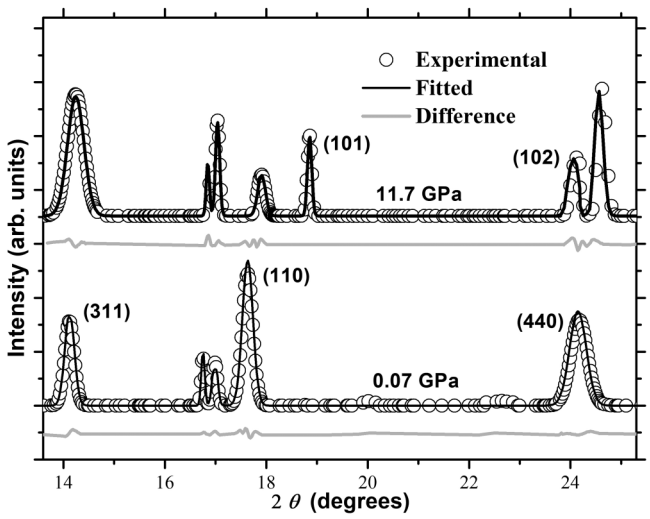

FIG. 5. The XRD patterns of Fe-filled SWCNHs at 0.07 and 11.7 GPa using Rietveld fitting.

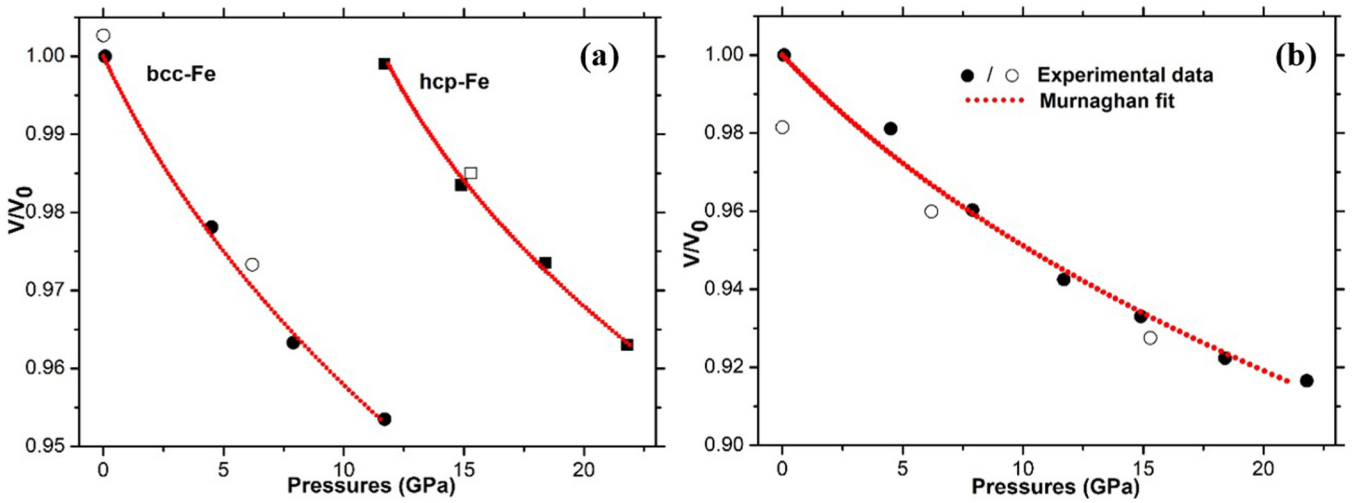

FIG. 6. Volume compression V/V_0 of nanocrystalline of (a) bcc Fe and hcp Fe confined by SWCNHs and (b) Fe_3O_4 confined by SWCNHs. The experimental data for hydrostatic compression are represented by the filled symbols while the open symbols represent data taken upon decompression. The red lines are fitted by the Birch–Murnaghan equation. V_0 is the reference volume and V is the deformed volume.

pressure, the *d*-spacing of the (440) plane decreased more rapidly than that of the (311) plane, suggesting that deformation along the direction of the (440) plane occurred more easily than that along the (311) plane.

The pressure-induced variation in the parameters of the lattice was obtained by analyzing the synchrotron diffraction patterns with the help of Le-Bail profile fitting.[22] To ensure the accuracy of the results, we also used the pressure dependencies of the *d*-spacing to calculate the lattice parameters and obtained similar to those of Le-Bail profile fitting. The pressure–volume (P–V) behaviors of Fe confined by the SWCNHs are shown in Fig. 6(a). When they were fitted to the Murnaghan equation of state,[25,26] we obtained the bulk modulus $B_0 = 153 \pm 25$ GPa and the derivative of the bulk modulus $B_0' = 22.6 \pm 10$. These results indicate that the compressibility of bcc Fe in the nanocrystalline form was slightly larger than that of bulk bcc Fe (B = 162.5 GPa).[27] With respect to the phase of hcp Fe, B_0 and B_0' had values of 163 ± 27 GPa and 33 ± 15, respectively, in the experimental results. Its bulk modulus was smaller than that had been determined earlier ($B_0 = 219 \pm 11$ GPa with $B_0' = 1$).[6] The high-pressure behavior of nanocrystalline Fe_3O_4 confined by SWCNHs was similar to the behavior of bulk Fe_3O_4, yielding $B_0 = 154 \pm 23$ and $B_0' = 11 \pm 5$ (Table I).[23,24] Furthermore, after decompression, the crystallite size of Fe_3O_4 was smaller than that of the initial unit cell as shown in Fig. 6(b), suggesting that lattice relaxation in nanocrystalline Fe_3O_4 led to irreversible change.

It is widely known that the main diffraction peak of carbon materials is formed owing to the (002) interlayer spacing derived from the layered graphitic structure.[28] In our case, the (002) *d*-spacing was due to interlayer spaces of graphene sheets in the core of the SWCNHs. The *d*-spacing decreased sharply at 3–5 GPa as illustrated in Fig. 7, where this can be attributed to the deformation of each CNH on the SWCNH surface. The cross section of individual CNHs underwent a transformation from circular to oval at 3.5 GPa.[10] In this way, the graphene sheets located at the core of the SWCNHs could be controlled by the hydrostatic pressure, and the *d*-spacing decreased significantly. Above 7 GPa, the *d*-spacing became stable at 0.302 nm. Up to 18 GPa, the peak intensity weakened and then nearly disappeared, suggesting that the core of the few layers of graphene sheets had buckled or crumpled, resulting in a loss of the diffraction signal.[29] These results were consistent with those of planar carbon, including graphite and graphene.[30] No structural transition occurred in this pressure range below 20 GPa. These results are in sharp contrast to those for Fe-filled CNTs, which underwent a sharp change at 9 GPa.[4]

TABLE I. Comparison of values of B_0 and B_0' of the bulk and nanocrystalline bcc Fe, hcp Fe, and Fe_3O_4 confined by SWCNHs (the value of B_0 of the nanocrystalline Fe_3O_4 is reported for rare).

Samples	B_0 (GPa)	B_0'
Bulk Fe	162.5	5.5[27]
Fe (bcc) confined by MWCNTs	167	8.5[5]
Fe nanowire confined by CNTs (with interfacial Fe_3C)	89.7	20[4]
Bulk Fe_3O_4	187	3[24]
Nanocrystalline (hcp) Fe	179 ± 8	3.6 ± 0.7[7]
Fe (bcc) confined by SWCNHs	153 ± 25	22.6 ± 10 (this study)
Fe (hcp) confined by SWCNHs	163 ± 27	33 ± 15 (this study)
Fe_3O_4 (bcc) confined by SWCNHs	154 ± 23	11 ± 5 (this study)

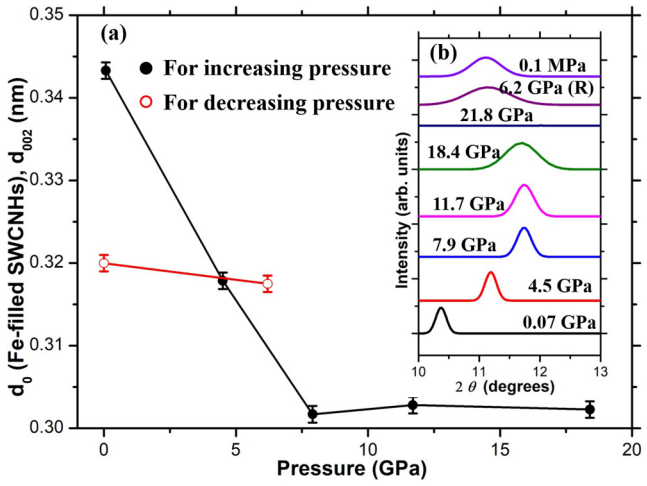

FIG. 7. (a) Variation in the average d-spacing (002) of Fe-filled SWCNHs with pressure. (b) Synchrotron XRD patterns of SWCNHs at different pressures.

IV. CONCLUSION

This study examined the high-pressure behavior of Fe confined by SWCNHs and Fe-filled SWCNHs produced by the one-step arc-discharge method. We used the Rietveld analysis with GSAS software and XPS analysis and found that the nanocrystalline Fe included 52% of bcc Fe, 47% of Fe_3O_4, and 1% of Fe_3C. The bcc Fe confined by the SWCNHs underwent a transition to hcp Fe, which was then completely converted back into bcc Fe at 6.2 GPa. This was different from Fe confined by CNTs owing to the effect of the special tubular confinement of the CNHs. The pressure of the encapsulated bcc Fe at phase transition was between that of the bulk Fe and nanocrystalline Fe. Importantly, bcc Fe and hcp Fe coexisted over a wide range of pressures. Fe_3O_4 confined by the SWCNHs did not undergo any structural transformation in pressures ranging from 0.07 to 21.8 GPa. Moreover, the bulk moduli of nanocrystalline bcc Fe, hcp Fe, and Fe_3O_4 confined by SWCNHs were lower than those of their large-grained counterparts.

ACKNOWLEDGMENTS

The authors appreciate Professor Noriaki Sano's help for synthesizing the Fe-filled SWCNHs. This work was funded by China Postdoctoral Science Foundation (Grant No. 2020M683671XB).

AUTHOR DECLARATIONS

Conflict of Interest

There authors have no conflicts to disclose.

DATA AVAILABILITY

The data that support the findings of this study are available from the corresponding author upon reasonable request.

REFERENCES

[1]S. Karmakar, P. K. Tyagi, D. S. Misra, and S. M. Sharma, Phys. Rev. B **73**, 184119 (2006).
[2]S. Karmakar, S. M. Sharma, M. K. Mukadam, S. M. Yusuf, and A. K. Sood, J. Appl. Phys. **97**, 054306 (2005).
[3]B. Li, Y. L. Nan, Y. Hu, X. Zhao, X. L. Song, H. N. Li, and L. Su, J. Phys. Chem. C **122**, 6976 (2018).
[4]S. Karmakar, M. Surinder, P. V. Sharma, Teredesai, and A. K. Sood, Phys. Rev. B **69**, 165414 (2004).
[5]H. K. Poswal, S. Karmakar, P. K. Tyagi, D. S. Misra, E. Busetto, S. M. Sharma, and A. K. Sood, Phys. Status Solidi B **244**, 3612 (2007).
[6]A. Dewaele, C. Denoual, S. Anzellini, F. Occelli, M. Mezouar, P. Cordier, S. Merkel, M. Veron, and E. Rausch, Phys. Rev. B **91**, 174105 (2015).
[7]B. Chen, D. Penwell, M. B. Kruger, A. F. Yue, and B. Fultz, J. Appl. Phys. **89**, 4794 (2001).
[8]S. Iijima, M. Yudasaka, R. Yamada, S. Bandow, K. Suenaga, F. Kokai, and K. Takahashi, Chem. Phys. Lett. **309**, 165 (1999).
[9]J. X. Xu, H. Tomimoto, and T. Nakayama, Carbon **49**, 2074 (2011).
[10]Y. L. Nan, B. Li, X. Zhao, X. L. Song, and L. Su, Carbon **125**, 236 (2017).
[11]B. Li, Y. L. Nan, X. Zhao, X. L. Song, H. Li, J. Wu, and L. Su, Appl. Phys. Lett. **111**, 221905 (2017).
[12]K. Urita, Y. Shiga, T. Fujimori, T. Iiyama, Y. Hattori, H. Kanoh, T. Ohba, H. Tanaka, M. Yudasaka, S. Iijima, I. Moriguchi, F. Okino, M. Endo, and K. Kaneko, J. Am. Chem. Soc. **133**, 10344 (2011).
[13]N. Sano, D. Himara, and H. Tamon, Chem. Eng. J. **271**, 43 (2015).
[14]C. Poonjarernsilp, N. Sano, N. Sawangpanich, T. Charinpanitkulc, and H. Tamon, Green Chem. **16**, 4936 (2014).
[15]A. P. Hammersley, S. O. Svensson, M. Hanfland, A. N. Fitch, and D. Hauserman, High Pressure Res. **14**, 235 (1996).
[16]A. C. Larson and R. B. Von Dreele, "General structure analysis system (GSAS)," Los Alamos National Laboratory LAUR Publication (1998).
[17]X. Xu, W. Yang, Y. Li, Z. Tu, S. Wu, and X. Ma, Chem. Eng. J. **267**, 289 (2015).
[18]J.-S. Li, S.-L. Li, Y.-J. Tang, M. Han, Z.-H. Dai, J.-C. Bao, and Ya.-Q. Lan, Chem. Commun. **51**, 2710 (2015).
[19]P. C. J. Graat and M. A. J. Somers, Appl. Surf. Sci. **100–101**, 36 (1996).
[20]M. Descostes, F. Mercier, N. Thromat, C. Beaucaire, and M. Gautier-Soyer, Appl. Surf. Sci. **165**, 288 (2000).
[21]D. Wilson and M. A. Langell, Appl. Surf. Sci. **303**, 6 (2014).
[22]A. C. Larson and R. B. Von Dreele, Los Alamos National Laboratory Report LAUR **86**, 748 (2004).
[23]S. Ju, T. Y. Cai, H.-S. Lu, and C.-De Gong, J. Am. Chem. Soc. **134**, 13780 (2012).
[24]D. R. Wilburn and W. A. Bassett, High Temp. High Press. **9**, 35 (1977).
[25]F. Birch, J. Geophys. Res. **83**, 1257, https://doi.org/10.1029/JB083iB03p01257 (1978).
[26]R. Angel, "Equations of state," in *High-Temperature and high-Pressure Crystal Chemistry*, edited by R. T. Downs (Reviews in Mineralogy, Mineralogical Society of America, 2000), Vol. 41, pp. 35–60.
[27]T. Takahashi, W. A. Bassett, and H.-K. Mao, J. Geophys. Res. **73**, 4717, https://doi.org/10.1029/JB073i014p04717 (1968).
[28]S. Bandow, F. Kokai, K. Takahashi, M. Yudasaka, L. C. Qin, and S. Iijima, Chem. Phys. Lett. **321**, 514 (2000).
[29]S. M. Clark, K.-J. Jeon, J.-Y. Chen, and C.-S. Yoo, Solid State Commun. **154**, 15 (2013).
[30]W. L. Mao, H.-K. Mao, P. J. Eng, T. P. Trainor, M. Newville, C.-c. Kao, D. L. Heinz, J. Shu, Y. Meng, and R. J. Hemley, Science **302**, 425 (2003).